J|A|C|S
ARTICLES

Published on Web 12/08/2008

Rapid, Solution-Based Characterization of Optimized SERS Nanoparticle Substrates

Ted A. Laurence,*,† Gary Braun,‡ Chad Talley,† Adam Schwartzberg,† Martin Moskovits,‡ Norbert Reich,‡ and Thomas Huser§

Chemistry, Materials, Earth and Life Sciences Directorate, Lawrence Livermore National Laboratory, Livermore, California 94550, Department of Chemistry and Biochemistry, University of California, Santa Barbara, California 93106, and Department of Internal Medicine, and NSF Center for Biophotonics Science and Technology, University of California, Davis, Sacramento, California 95817

Received August 7, 2008; E-mail: laurence2@llnl.gov

Abstract: We demonstrate the rapid optical characterization of large numbers of individual metal nanoparticles freely diffusing in colloidal solution by confocal laser spectroscopy to guide nanoparticle engineering and optimization. We use ratios of the Rayleigh and Raman scattering response and rotational diffusion timescales of individual nanoparticles to show that hollow gold nanospheres and solid silver nanoparticle dimers linked with a bifunctional ligand, both specifically designed nanostructures, exhibit significantly higher monodispersity than randomly aggregated gold and silver nanoparticles.

Introduction

Interest in surface-enhanced Raman spectroscopy (SERS) has increased greatly in recent years after Raman experiments at the single molecule level using surface-enhanced resonance Raman spectroscopy (SERRS) were reported.[1,2] This development reinvigorated interest in SERRS and SERS as ultrasensitive biosensing platforms. Although the SERS phenomenon has been understood qualitatively for a long time,[3] its application is limited by our ability to engineer structures whose properties can be quantitatively determined and predicted. Even given the considerable progress in forming designed nanostructures such as nanoshells,[4] metal films over nanospheres (FONs),[5] nanorings[6] and others, this significant goal is still largely unrealized. A key factor slowing progress is the absence of quantitative, statistically significant data that address questions of SERS signal uniformity in ensembles of purportedly identically fabricated SERS substrates. The absence of a reliable methodology for producing such data sets has also hampered the development of universally accepted performance criteria in terms of which the SERS enhancement, uniformity and reproducibility of SERS substrates can be assessed.

Currently, characterization of SERS-active substrates is rather inefficient, normally interrogating immobilized particles one by one. Multimodal approaches are often used, where single particle spectra and intensity are correlated with transmission electron microscopy (TEM), scanning electron microscopy (SEM) or atomic force microscopy (AFM) to determine their size and shape; see, for example.[7,8] Most studies present data from only a handful of nanoparticles or nanoparticle clusters (sometimes just 3−4), and only in rare cases up to ∼100 nanoparticles are probed. Although sufficient for demonstrating the potential for SERS in applications, these studies only touch on issues of uniformity.

Here, we describe an efficient and rapid way to obtain such data, and demonstrate the power of our approach by comparing commonly used colloidal nanoparticle-based SERS substrates to more recently developed, nanoengineered structures. The approach allows for the characterization of multiple parameters of individual SERS-active colloidal nanoparticles in suspension. We characterize the spectroscopic properties of various nanoparticle systems, freely diffusing in solution, using single particle SERS intensity and correlation-spectroscopy techniques. Nanoparticles are compared in particle size, polarization response, Raman, Rayleigh, and continuum background—all parameters which are acquired simultaneously. Similar to other solution-based studies such as single-molecule fluorescence (SMF),[9] this technique is limited only by the number of acquisition channels. Signals obtained from thousands of particles are collected within a short time as they diffuse into and out of the laser spot, enabling statistical evaluations and characterization of subpopulations.[10] Correlation techniques have been used for many years in fluorescence studies to characterize mobility, rotational

† Lawrence Livermore National Laboratory.
‡ University of California, Santa Barbara.
§ University of California, Davis.

(1) Kneipp, K.; Yang, W.; Kneipp, H.; Perelman, L. T.; Itzkan, I.; Dasari, R. R.; Feld, M. S. *Phys. Rev. Lett.* **1997**, *78* (9), 1667–1670.
(2) Nie, S.; Emory, S. R. *Science* **1997**, *275* (5303), 1102–1106.
(3) Moskovits, M. *Rev. Mod. Phys.* **1985**, *57* (3), 783–826.
(4) Oldenburg, S. J.; Averitt, R. D.; Westcott, S. L.; Halas, N. J. *Chem. Phys. Lett.* **1998**, *288* (2−4), 243.
(5) Freunscht, P.; Van Duyne, R. P.; Schneider, S. *Chem. Phys. Lett.* **1997**, *281* (4−6), 372.
(6) Aizpurua, J.; Hanarp, P.; Sutherland, D. S.; Käll, M.; Bryant, G. W.; García de Abajo, F. J. *Phys. Rev. Lett.* **2003**, *90* (5), 057401.
(7) Schwartzberg, A. M.; Oshiro, T. Y.; Zhang, J. Z.; Huser, T.; Talley, C. E. *Anal. Chem.* **2006**, *78* (13), 4732–4736.
(8) Talley, C. E.; Jackson, J. B.; Oubre, C.; Grady, N. K.; Hollars, C. W.; Lane, S. M.; Huser, T. R.; Nordlander, P.; Halas, N. J. *Nano Lett.* **2005**, *5* (8), 1569–1574.
(9) Weiss, S. *Science* **1999**, *283* (5408), 1676–1683.
(10) Dahan, M.; Deniz, A. A.; Ha, T.; Chemla, D. S.; Schultz, P. G.; Weiss, S. *Chem. Phys.* **1999**, *247* (1), 85–106.

 10.1021/ja806236k CCC: $40.75

diffusion, molecular interactions, and photophysical fluctuations, and are here extended to SERS-active nanoparticles. Specifically, our experiments using SERS are similar in methodology to those conducted by Eggeling et al.,[11] but with the addition of multiple channels monitoring narrow spectral ranges and the omission of the lifetime spectroscopy. In order to determine the benefits of nanoengineering on SERS uniformity, we compare a series of metallic nanoparticle preparations. We compare the SERS response from randomly aggregated polydisperse silver (Ag) nanoparticles and solid spherical gold (Au) nanoparticles of uniform size with nanoengineered structures: linked clusters of the polydisperse Ag nanoparticles and uniform hollow gold nanospheres. A strong dependence of scattering particles on shape and structure is observed and we conclude that a superior monodispersity in SERS response is obtained from the nanoengineered structures versus samples made using random aggregation.

Materials and Methods

Four substrates are used and compared quantitatively for our scattering measurements (further details are in the Supporting Information). First, solid Ag nanoparticles with a wide variety of sizes and shapes (typically 30−60 nm in diameter) are produced using the citrate reduction procedure from Lee and Meisel.[12]

Second, the Au particles were made via the seed mediated growth method of Jana et al.[13] The resulting sol contained approximately 50 nm Au particles with good homogeneity. These produce stronger signals than commercial preparations, likely due to a greater propensity for clustering or aggregation.

Third, hollow Au particles were produced by the same method as published previously.[7] The peak of the plasmon resonance was near 600 nm, and the size of the nanoparticles was shown by TEM to be near 45 nm.

Fourth, the ∼50 nm diameter Ag nanoparticles of Lee and Meisel[12] were formed into clusters using a linker molecule. First, the nanoparticles were concentrated by centrifugation to twice the concentration in 10 mM sodium phosphate buffer pH 7.8. ABT in methanol (160 μM) was added to induce aggregation and caused a color change from yellow to green (requiring ∼3 μM ABT) followed by addition of 20 μL 1 mg/mL poly(*N*-vinylpyrrolidone-co-acrylic acid) potassium salt (M_n 18 000, AK 2 mol%, Polymer Source Inc., PVPA) in water. Five minutes later two rounds of low speed centrifuging and redispersion in water were performed, each time discarding the yellow supernatant and any solids. The size distribution (by TEM) was centered near 100 nm.

Optical characterization experiments are performed on the samples as prepared, without dilution. No specific Raman signal is found for the raw nanoparticle samples except for the ABT linked clusters. In order to achieve a specific Raman signal from the pure nanoparticles we added 10 μM or 50 μM 4-mercaptobenzoic acid (MBA) as indicated, and 50−500 μM for the Au nanospheres due to their higher concentration. These were allowed to incubate at room temperature for 1−2 h.

Ratiometric Spectroscopy of Single Nanoscatterers. Individual light-scattering nanoparticles or small clusters of nanoparticles are allowed to diffuse freely in solution through the confocal detection volume defined by the experimental setup described in Figure 1a. Linearly polarized excitation light from a 633 nm HeNe laser is reflected by a dichroic mirror (DM1), and focused into solution by a high numerical aperture microscope objective (60× 1.4 NA oil immersion Plan Apochromat, Nikon). Collected light is transmitted

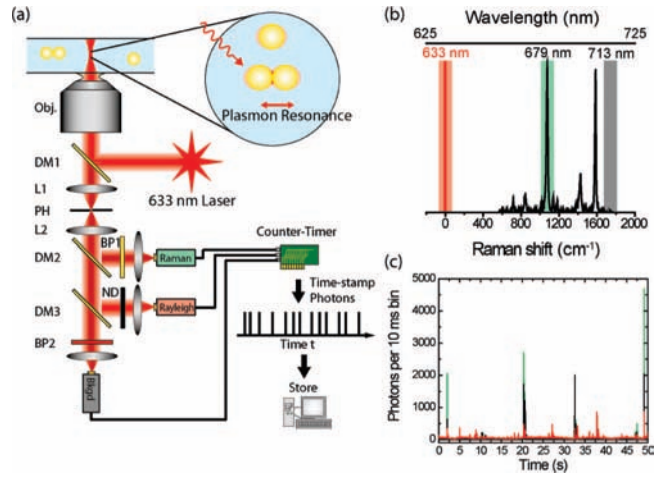

Figure 1. Homogeneity of size and optical response of metal nanoparticles is probed using solution-based ratiometric single particle and cluster spectroscopy. (a) Experimental setup. Individual metallic nanoparticles and clusters of nanoparticles are allowed to freely diffuse in solution. Bursts of photons scattered by nanoparticle clusters diffusing through the laser focus are collected and split into three spectral domains isolating the 1055 cm^{-1} benzene ring breathing Raman line of 4-mercaptobenzoic acid (MBA; green detector), the continuum background (gray detector), and Rayleigh scattered light from the particles (red detector). 4-aminobenzenethiol (ABT) used for the polymer-coated nanoclusters has a similar Raman mode. Photons are timed and stored in a computer. (b) SERS spectrum of MBA on Ag nanoparticles overlaid with spectral ranges selected by filters for the three detectors. (c) Time trace with 10 ms time resolution showing individual Au nanoparticle scattering centers traversing the optical detection volume. Colors correspond to the three channels in part (a).

through DM1, focused by lens L1, spatially filtered by confocal pinhole (PH), and collimated by lens L2. Two dichroic mirrors (DM2 and DM3) split the scattered light into three spectral domains. BP1 (679DF6, Omega Optical) selects the 1055 cm-1 benzene ring Raman mode of 4-mercaptobenzoic acid (MBA; green detector); ABT has a similar Raman mode. BP2 (713DF6, Omega Optical) selects a small spectral region without any Raman line for MBA (gray detector); this channel monitors the strength of the continuum background. A third channel has an OD 3.6 neutral density filter and monitors the Rayleigh scattering (red detector).

Photons detected by avalanche photodiodes (APDs, SPCM-AQR-14, PerkinElmer Optoelectronics) send TTL pulses to the counter timer card (PCI-6602, National Instruments), which records them with 12.5 ns time resolution.

Analysis of Photon Bursts. A burst of scattered photons from individual scattering clusters or particles is found using the algorithm described in ref 14 which provides start and end times t_{start} and t_{end}. The count rates, I_{Rm} (Raman), I_{Ry} (Rayleigh), and I_{Bkgd} (continuum background), are averaged over each bursts, after subtracting a baseline background for each channel. This baseline is found by calculating the median of the 100 time bins (of 10 ms width) before the burst. Note that the Rayleigh scattering APD has a neutral density filter added with OD 3.6 and has further attenuation due to the dichroic mirrors, and that the Raman channel can also contain a contribution from continuum background scattering, because of its broad spectrum, so that I_{Rm} is not 0 in the absence of a Raman-active molecule.

Correlation Spectroscopy. Correlation spectroscopy of individual photon bursts is performed as described in ref 14 Correlation spectroscopy on SERS, background scattering, and Rayleigh scattering signals of nanoparticles provides rotational and translational diffusion parameters of particles. These can be interpreted in terms of the size of the scattering particles or clusters. The

(11) Eggeling, C.; Schaffer, J.; Seidel, C. A. M.; Korte, J.; Brehm, G.; Schneider, S.; Schrof, W. *J. Phys. Chem. A* **2001**, *105* (15), 3673–3679.
(12) Lee, P. C.; Meisel, D. *J. Phys. Chem.* **1982**, *86* (17), 3391–3395.
(13) Jana, N. R.; Gearheart, L.; Murphy, C. J. *Chem. Mater.* **2001**, *13* (7), 2313–2322.
(14) Laurence, T. A.; Kwon, Y.; Yin, E.; Hollars, C. W.; Camarero, J. A.; Barsky, D. *Biophys. J.* **2007**, *92* (6), 2184–2198.

presence or absence of a rotational diffusion component will also allow us to distinguish between anisotropic scattering from particle−particle junctions and the more isotropic scattering from individual nanospheres.

The following model was used to fit the individual correlations:

$$C(\tau) = c\left\{1 + \frac{1}{N(1+\tau/\tau_D)}\left[1 + \frac{A_P}{1-A_P}\exp(-\tau/\tau_P)\right]\right\} \quad (1)$$

τ_D is the translational diffusion time, τ_P is the rotational diffusion time, and A_P is the relative amplitude of the rotational diffusion component. N is the number of particles in the detection volume, and c is a correction factor required to fit the correlations from individual particles.[14]

Results

Ratiometric Single Cluster Spectroscopy Monitors Homogeneity of SERS Response. To gauge the SERS intensity and uniformity from engineered nanoparticle systems we employ two ratiometric variables calculated from each photon burst event (each burst corresponds to an individual nanoparticle or nanoparticle cluster). First, I_{Rm}/I_{Ry} compares the number of Raman scattered photons to those from Rayleigh scattering. This ratio compares the intensity of SERS from adsorbed molecules to the Rayleigh 'cross section', and is affected by size, shape, resonance, and polarization conditions of the nanoparticles. Second, I_{Rm}/I_{bkgd} compares the number of photons that are due to molecular SERS scattering to the continuum background, generally attributed to scattering[15,16] or luminescence[17] from the metal in a SERS active material. Both ratios increase upon functionalization of the nanoparticles with MBA or ABT due to the onset of SERS. Aggregation of bare Au and Ag nanoparticles caused by addition of NaCl increased I_{Rm}/I_{Ry}, but not I_{Rm}/I_{bkgd} (data not shown); these results are indicative of an increased continuum background caused by aggregation, but no Raman scattering signal. The two-dimensional histograms in Figure 2 show the number of photon bursts as a function of these ratios for the cases of solid Ag, solid Au, Au nanosphere, and linked Ag particle samples. For all the nanoparticle preparations that did not initially contain a Raman probe (all but the linked Ag particles), we first characterized the light scattering properties of the bare particles, then we added enough MBA to maximize the Raman signal without inducing large-scale aggregation (as evidenced by color change and correlation analysis).

The solid Ag and Au samples exhibit two populations with addition of 10 μM MBA which causes moderate aggregation and SERS intensity: a strongly Raman-active population ("strong SERS population" upper right of Figure 2b−c) and a weakly Raman-active population ("weak SERS population" bottom middle of Figure 2b−c). The Ag nanoparticles used in this study are not of uniform size or shape, but they have been frequently used in studies showing very large Raman enhancements.[1,2,15] The Au nanoparticles are of much more uniform size and shape than Ag nanoparticles, as evidenced by transmission electron microscopy (data not shown). Note that, in the strong SERS populations, the ratio I_{Rm}/I_{bkgd} is lower for Au than for Ag, consistent with previous observations that Ag in general provides larger SERS enhancements.[3] In the case of the larger aggregates

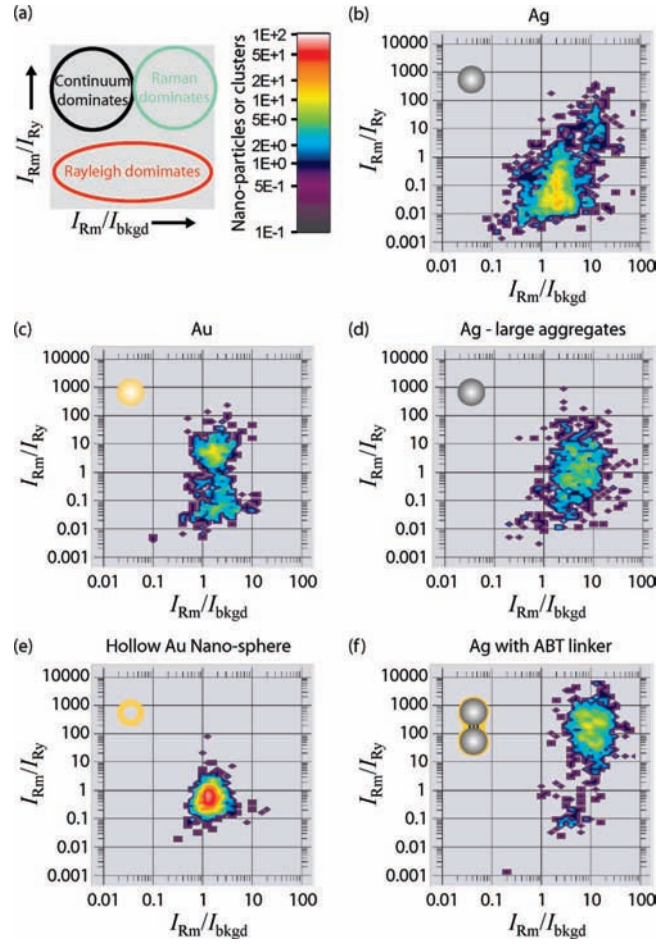

Figure 2. Two-dimensional histograms of single nanoparticles or clusters compare strengths of Raman scattering, Rayleigh scattering, and the continuum background signal. Ratiometric variables I_{Rm}/I_{Ry} and I_{Rm}/I_{bkgd} calculated for single diffusing clusters or particles are used to monitor the effects of functionalizing the nanoparticles with 4-mercaptobenzoic acid (MBA). (a) The ratio I_{Rm}/I_{Ry} compares the strength of the Raman scattering to the Rayleigh scattering (Rayleigh scattering is attenuated by a neutral density filter). The ratio I_{Rm}/I_{bkgd} compares the strength of the Raman scattering to the continuum background. Histograms are shown for: (b) Ag nanoparticles with 10 μM MBA; (c) Au nanoparticles with 10 μM MBA; (d) Ag nanoparticles with 50 μM MBA, which induces large-scale aggregation; (e) Au nanospheres (45 nm) with 50 μM MBA (does not induce aggregation); and (f) Ag nanoparticles linked with ABT, and polymer coated.

(50 μM MBA, Figure 2d) we find only a single population with ratios that are intermediate between the two populations observed with 10 μM MBA.

The hollow Au nanospheres (Figure 2e) exhibit a much more homogeneous response when compared to the solid Au and Ag nanoparticles. There is only one peak, and the peak is narrower in the ratios I_{Rm}/I_{Ry} and I_{Rm}/I_{bkgd} than the random-aggregated nanoparticles.

By linking the solid Ag nanoparticles with a bifunctional linker, ABT (see Figure 2f), the distribution obtained was very different from those obtained with random aggregation. Almost all of the nanoparticle clusters are in the Raman-active subpopulation, although there remains a very small, less Raman-active subpopulation. The ratio I_{Rm}/I_{Ry} is higher than that obtained for any of the other systems studied, and the ratio I_{Rm}/I_{bkgd} obtained is centered at the highest value observed in randomly aggregated Ag.

(15) Jiang, J.; Bosnick, K.; Maillard, M.; Brus, L. *J. Phys. Chem. B* **2003**, *107* (37), 9964–9972.
(16) Otto, A.; Timper, J.; Billmann, J.; Kovacs, G.; Pockrand, I. *Surf. Sci.* **1980**, *92* (1), L55.
(17) Heritage, J. P.; Bergman, J. G.; Pinczuk, A.; Worlock, J. M. *Chem. Phys. Lett.* **1979**, *67* (2−3), 229.

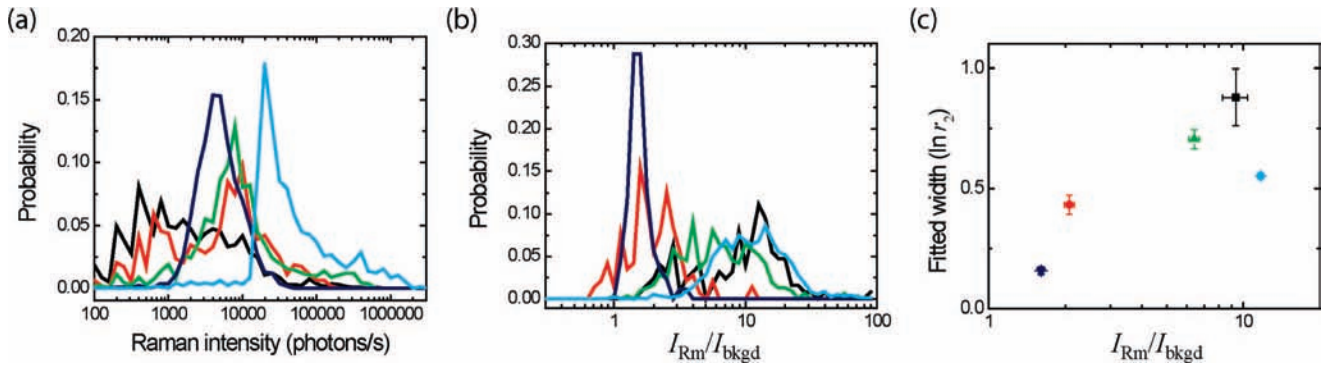

Figure 3. Raman scattering characteristics of the most strongly Raman-active populations for each type of nanoparticle. The data shown are taken from same data as Figure 2. Black: Ag nanoparticles with 10 μM MBA. Red: Au nanoparticles with 10 μM MBA. Green: Ag nanoparticles with 50 μM MBA. Blue: Au nanospheres with 50 μM MBA. Cyan: Ag nanoparticles linked with ABT, and polymer coated. (a) Histogram of Raman intensities found for the selected Raman line for the various nanoparticle samples. (b) Histograms of ratiometric variable I_{Rm}/I_{bkgd} calculated for single diffusing nanoparticles or clusters with bright Raman signal (>15 kHz). (c) Histograms in (b) were fitted to a log-normal distribution function. The resulting widths (in ln units) are plotted vs the mean peak position.

In Figure 3a, we compare the Raman intensities for these samples. The brightest distribution is obtained from the ABT-linked Ag nanoparticles, followed by the randomly aggregated Ag and Au nanoparticles. The dimmest structures on average are the hollow nanospheres.

In Figures 3b−c, we compare the homogeneity of these samples after selecting only the Raman-active subpopulations (those with I_{Rm} > 15 kHz). We plot in Figure 3b the normalized histograms of I_{Rm}/I_{bkgd} for each sample from Figure 2. We then fit each of the histograms in Figure 3b to a log-normal distribution to extract the mean and width of the fits, plotted in Figure 3c. The histogram width for the hollow nanospheres is the narrowest obtained for these samples. The histogram for the ABT-linked Ag nanoparticles is narrower than that for the subpopulation of Ag nanoparticles, but not by as much as the hollow nanospheres (the overall Raman intensity is much higher).

Scattering Anisotropy Monitored by Sensitivity to Laser Polarization. The temporal response of SERS from individual nanoparticles may be analyzed using SERS correlation spectroscopy, similar to fluorescence correlation spectroscopy (FCS).[11] Interestingly, the correlation response in SERS experiments on diffusing nanoparticles exhibits two characteristic time scales (see Figures 4a−c). The longer time scale is indicative of translational diffusion of the nanoparticles through the confocal detection volume, and the shorter time scale is due to rotational diffusion of the nanoparticles. The rotational diffusion is only visible if the plasmon resonance of the nanoparticle is preferentially excited along a certain direction—a scattering anisotropy. Such a preferred direction may arise due to varying shapes of particles or by particle aggregation, e.g. dimer formation. For truly spherically symmetric particles, no sensitivity to polarization is expected.

When the laser excitation is polarized along the preferred dipole axis of a Ag nanoparticle or nanoparticle cluster, a larger scattering signal is observed, whereas it is much weaker if the laser beam is polarized perpendicular to the preferred dipole (Figure 4b). To identify the different diffusion time scales we split the emission into two channels with perpendicular polarizations, and monitored the fluctuation time scales by performing auto- and cross-correlations between the two signals (Figure 4c). For the shorter time scale, the autocorrelations of both polarizations had amplitudes larger than for the cross-correlations. This indicates a polarization-sensitive fluctuation from rotational diffusion of the nanoparticles. A similar identification of rotational diffusion was previously found with Ag nanoparticles.[11] Having identified the translational and rotational diffusion components, we now analyze the heterogeneity of the sample on a particle-by-particle basis.

The nanoparticle samples we studied show different characteristics when monitored with correlation spectroscopy. By applying recently developed single-molecule FCS analysis methods[14] to SERS we can determine the correlations from individual nanoparticles and nanoparticle clusters. It further allows us to perform a statistical analysis of the results obtained from many individual scattering centers, rather than averaging the response of all particles into a single correlation plot. In Figures 4d−f we show examples of the autocorrelation function of the Rayleigh (red) and the Raman (black) channels as well as their cross-correlations (green and blue) for individual nanoparticles or nanoparticle clusters. Figure 4d shows typical results for Ag nanoparticle clusters. Interestingly, both the Raman (black) and Rayleigh (red) channel autocorrelations show strong rotational diffusion contributions, and the cross-correlations show similar contributions, indicating that the Rayleigh and Raman dipoles are well aligned with respect to each other. Results for the Ag nanoparticles linked with ABT are similar in appearance to those found using the randomly aggregated nanoparticles, except that they occur at longer timescales. In all cases, autocorrelations and cross-correlations of the Raman and continuum channels overlap within expected error (data not shown). This agrees with previous observations that the continuum background and Raman signals appear to turn on and turn off together.[15]

As shown in Figure 4e, Au nanoparticles exhibit a different behavior. First, the amplitudes of the rotational diffusion components are smaller than for the Ag nanoparticles. Second, the polarization component of the cross-correlations often have negative amplitudes (seen as a dip in the cross-correlation at shorter time interval), indicating that the preferred axes for Rayleigh and Raman scattering may not overlap.

Hollow Au nanospheres exhibit another, very distinctive behavior (Figure 4f). Here, the rotational diffusion component of scattering is not detectable. This is indeed the expected behavior for isolated (nonaggregated) spherically symmetric nanoparticles.

Sizing Nanoparticles Using Rotational Diffusion Time. By analyzing single burst correlations, such as the ones shown in

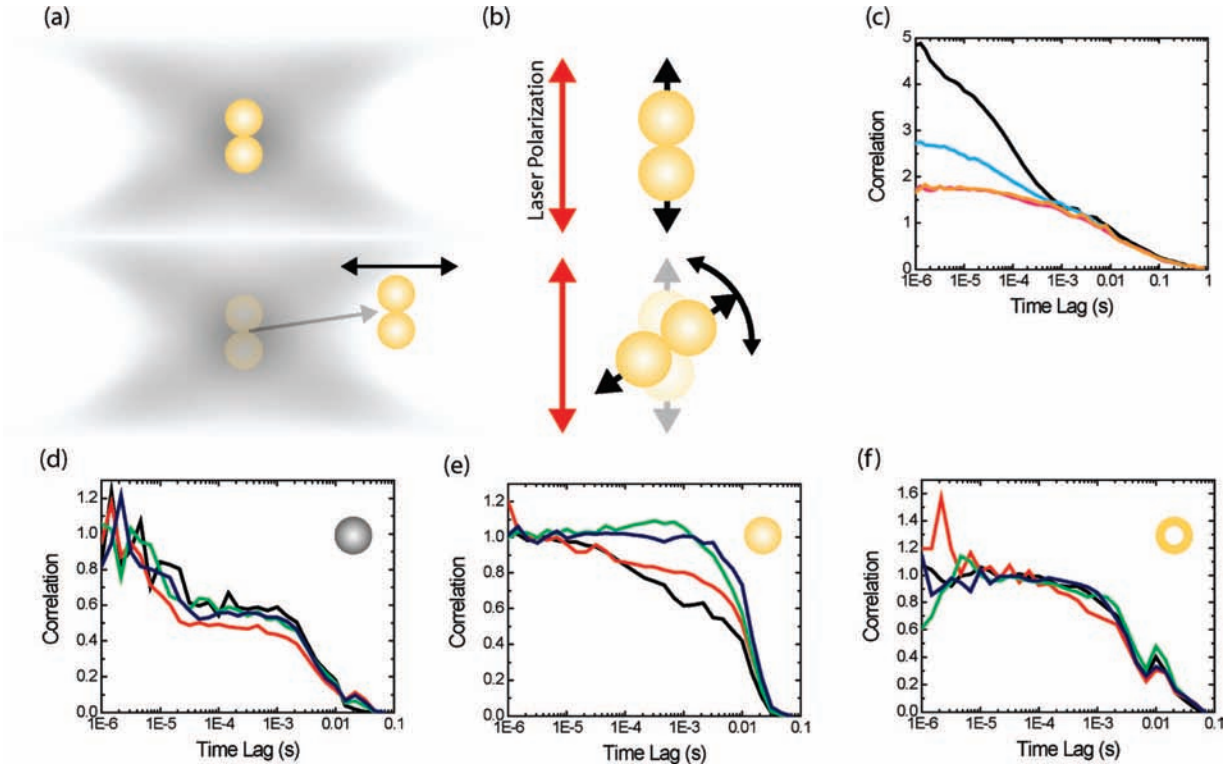

Figure 4. Translational diffusion and rotational diffusion both affect correlation spectroscopy signals of Rayleigh and Raman scattering. (a) Translational diffusion of nanoparticles into and out of the confocal detection volume produces intensity fluctuations. (b) Rotational diffusion of polarization-sensitive nanoparticle clusters produces intensity fluctuations. The time scale of fluctuations induced by translational diffusion depends on the size of confocal detection volume, but the (shorter) time scale for rotational diffusion does not. (c) These two time scales are evident in correlations of Raman scattering signals from nanoparticles diffusing in solution, and are identified using a modified experimental setup with polarization sensitive detection (monitoring channels parallel and perpendicular to the excitation polarization). Autocorrelations of the parallel (black) and perpendicular (cyan) channels are shown, as well as cross-correlations of the two channels (orange and magenta). (d-f) Representative correlations from *single bursts* are shown after expanding the correlation region. (d) Correlations for a single Raman active Ag scattering center. Autocorrelation of Raman signal (black), autocorrelation of Rayleigh signal (red), and the two cross-correlations of the Raman signal with the Rayleigh signal (green and blue) are shown. (e) Correlations for single Raman-active Au scattering center. (f) Correlations for single Au nanosphere. For hollow nanospheres, the rotational diffusion fluctuations are absent due to their isotropic surface plasmon response.

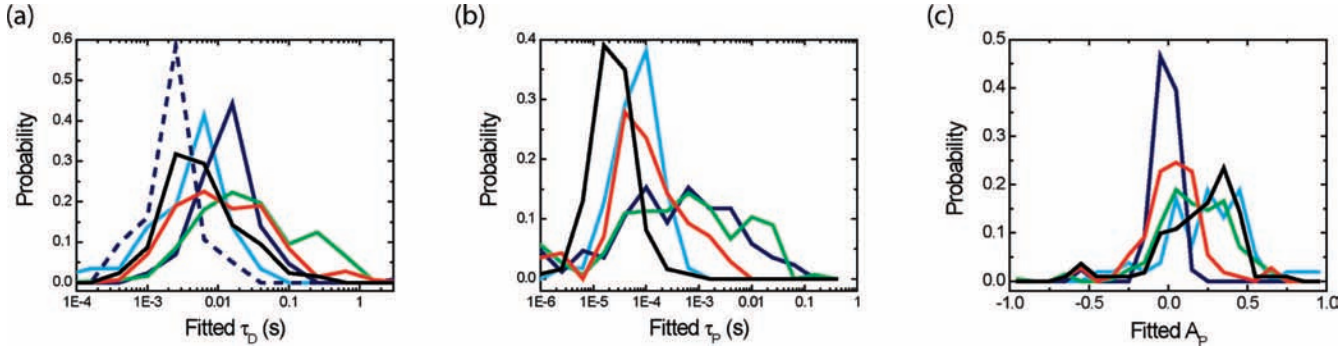

Figure 5. For each scattering center, a two component correlation spectroscopy model is fitted to the correlations from an individual burst of photons. It is a global fit of all four correlations shown in figure 4. The results are formed into histograms shown here, and the populations are fitted. The data shown are extracted from nanoparticles or clusters with bright Raman signal as selected in Figure 3b. Black: Ag nanoparticles with 10 μM MBA. Red: Au nanoparticles with 10 μM MBA. Green: Ag nanoparticles with 50 μM MBA. Blue: Au nanospheres with 50 μM MBA. Cyan: Ag nanoparticles linked with ABT, and polymer coated. (a) Histograms of fitted translational diffusion time τ_D. The dotted blue line shows histogram of τ_D for the Au nanosphere using fits without a rotational diffusion component—performing fits with two time scales where only one was needed caused τ_D to shift to higher values (solid blue line). (b) Same as (a), but now for histograms of fitted rotational diffusion time τ_P. (c) Histograms of the rotational diffusion amplitude A_P from the cross-correlation; the use of the cross-correlation amplitude reduces artifacts found by only using autocorrelations. A_P measures the strength of the polarization-related fluctuations related to rotational diffusion. If A_P is larger than 0, then there was a significant component of the polarization-related fluctuation found. If A_P is less than 0, that component was negative, indicating that the Raman-active and Rayleigh-active dipoles are not aligned, or are nearly perpendicular.

Figure 4d−f, we can extract two size-related parameters: the translational diffusion and rotational diffusion time scales. Figure 5 shows histograms of single burst parameters obtained from many individually fitted particle burst correlations. For the translational diffusion times (Figures 5a), the 10 μM MBA Ag clusters have a faster diffusion times compared to both 10 μM

with Au and 50 μM with Ag (indicating smaller size). The Au solid and hollow nanosphere particles have very different diffusion times, despite their similar monomer diameters (~50 and 45 nm diameters, respectively), indicating aggregation of the solid Au. For Ag clusters with the highest MBA concentration of 50 μM, we observe much wider distributions of translational diffusion times.

The translational diffusion time depends on the diffusion constant according to,

$$\tau_D = \frac{\omega^2}{4D} = \frac{\omega^2 3\pi\eta}{4k_B T} l \quad (2)$$

The particle is assumed to be spherical, so that the diffusion constant is $D = k_B T/3\pi\eta l$. ω is the waist of the Gaussian confocal detection volume. η is the dynamic viscosity of water, and l is the diameter of the spherical particle. Hence the translational diffusion time can be used to size particles. However, the sizing depends on the size of the confocal detection volume which can vary due to alignment and must be carefully calibrated. More importantly, the diffusion time depends only linearly on diameter.

For the rotational diffusion times (Figure 5b), we again see that the Ag particles have the fastest diffusion. However, we are not able to obtain reliable rotational diffusion times for the hollow nanosphere sample since the rotation diffusion component is missing due to spherical symmetry. As seen in Figure 5c, the hollow nanosphere sample had values for A_P near 0, indicating a weak rotational diffusion component. In the other cases, significant and often strong rotational diffusion amplitudes were found (in some cases with negative cross-correlation amplitudes indicating nonaligned Rayleigh and Raman response). The dominant rotational diffusion time depends on the rotational diffusion constant Θ according to,

$$\tau_P = \frac{1}{6\Theta} = l^3 \frac{\pi\eta}{6k_B T} \quad (3)$$

Again, the particle (or cluster) is assumed to be spherical, so that $\Theta = k_B T/\pi\eta l^3$. In general, rotational diffusion decays measured by correlation spectroscopy are multiexponential.[18] Even for a sphere, there are two time scales.[19] However, one time scale dominates for a sphere, and we use that here. In comparison to translational diffusion, the most important features are the much stronger dependence on size (cubic in diameter l, rather than linear), and the lack of dependence of confocal detection volume size.

We can use the rotational diffusion time to estimate the size of the particles, and do so assuming a spherical shape. We first performed simulations of 50 and 100 nm particles diffusing in solution (see Supporting Information) in order to model the cubic relationship between diffusion time and diameter. This function is plotted as a line in Figure 6 along with the mean size of each sample as determined from the data in Figure 5. The increase in size and variability is particularly evident in the Ag nanoparticle sample aggregated with 50 μM MBA. Furthermore, ABT-linked Ag clusters (cyan) appear to be similar in size to the solid Au aggregates (red) while exhibiting a mean Raman to Rayleigh ratio at least 10 times larger than Au. Notably, the diameter of the ABT clusters is consistent with that derived from TEM measurements, validating the technique for SERS active nanoparticle systems.

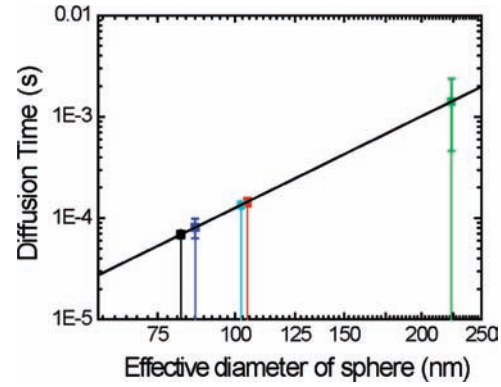

Figure 6. Average sizes of the samples used in Figure 5 are determined using their rotational diffusion time scales (color scheme is same as in Figure 5). For the Au nanospheres at 50 μM MBA, no strong rotational diffusion component was found. The value shown in blue is for 500 μM MBA and hollow nanospheres where some aggregation occurs, allowing for detection of the rotational diffusion from interparticle junctions.

Discussion

Effect of Nanoengineering on the Consistency and Intensity of SERS Signal. Current challenges in SERS-active nanostructure design include maximizing reproducibility and intensity. Two general routes are possible to improve upon the typically used, randomly aggregated nanoparticle samples. First, the individual nanoparticles may be engineered to have a consistent shape that has a strong plasmon resonance, such as the hollow nanospheres tested here[7] or nanoshells.[4] Second, given that interparticle junctions produce the strongest SERS signals, formation of those junctions can be precisely controlled, as done in forming the ABT-linked nanoclusters tested here. The results from the ratiometric variables clearly show that nanoengineered substrates have improved SERS homogeneity and intensity when compared to randomly aggregated SERS substrates. The polarization-induced fluctuation amplitudes and sizing verify that the results from the ratiometric data are from the samples as designed and as typically measured using TEM, SEM, or AFM.

The hollow Au nanospheres provided the narrowest distributions in the ratiometric variables by a significant margin (Figure 2). This statement holds even after selecting only the most SERS-active populations of each sample (Figure 3c). These observed bursts were indeed from individual nanospheres, as indicated by the lack of anisotropy in the scattering signals (Figure 4); only after enough MBA was added to start clustering was any anisotropy observed. These are especially encouraging results, verifying that designed nanostructures have improved upon random aggregation. Previous results showed that nanoshells and hollow nanospheres perform as nanoscale pH meters more consistently than random aggregates.[7,20] The current results extend those in two important aspects. First, previous analyses were obtained by searching for Raman-active nanoparticle clusters, which misses much of the heterogeneity seen here, with many nanoparticle clusters being weakly Raman-active. Second, we obtain results for ~1000 particles for several nanoparticle preparations under various conditions, which allows us to view the full statistical distributions of the scattering response rather

(18) Aragon, S. R.; Pecora, R. *J. Chem. Phys.* **1976**, *64* (4), 1791–1803.
(19) Aragón, S. R.; Pecora, R. *Biopolymers* **1975**, *14* (1), 119–137.
(20) Bishnoi, S. W.; Rozell, C. J.; Levin, C. S.; Gheith, M. K.; Johnson, B. R.; Johnson, D. H.; Halas, N. J. *Nano Lett.* **2006**, *6* (8), 1687–1692.

than simple means and widths of distributions. We conclude that the hollow nanospheres are more uniform than any other nanoparticle substrate, but they have a lower Raman activity than that obtained from random aggregation of nanoparticles.

By controlling the formation of interparticle junctions, the ABT-linked nanoclusters produce the most consistently intense SERS signals we measured. Although the size of the linked nanoparticle clusters is smaller than those obtained upon large-scale aggregation of the Ag nanoparticles (50 μM MBA), the signal intensities are stronger than any of the randomly aggregated samples. The less SERS-active population is much smaller than observed with the solid Ag and Au nanoparticles. This enriched distribution comes in part from the size selective centrifugation process. Although the shape and size of these nanoparticles are not completely uniform, their significantly more uniform response is likely obtained due to the efficient structure of linked dimers and the relationship between the number of adsorbates per hot spot, hot spots excited per nanoparticle, and nanoparticles per cluster. The dimers are in stark contrast to the larger, random aggregates composed of tens to hundreds of nanoparticles when using uncontrolled MBA and/or salt aggregation. For those large aggregates $I_{Rm}/I_{Ry}$is expected to vary with size and structure while only a fraction of hot spots is excited at any one time in a fractal-like structure.[21] Extrapolating from the relationships in Figure 3c we expect that controlled linking of more monodisperse Ag or Au would generate a mean I_{Rm}/I_{bkgd} value significantly larger than for 10 μM MBA but with a narrower distribution.

We note that using nanoengineering to produce consistently spherical nanoparticles did not significantly improve the reproducibility. The solid Au nanoparticles, which are spherical, did not perform better than the Ag nanoparticles, which have a variety of shapes and sizes.

Origin of Two Populations in Randomly Aggregated Solid Nanoparticles. The randomly aggregated solid Au and Ag nanoparticles exhibited two populations, one strongly SERS active, one weakly SERS active. A possible explanation for the presence of two populations for the Ag and Au nanoparticles is that the strong SERS population consists of clusters, and that the second, weak SERS population consists of monomers. Although we find that the weak SERS population for the Ag nanoparticles consists in part of nanoparticles or clusters of nanoparticles with strong polarization dependency (similar to the strong SERS population), we understand that the Ag nanoparticle monomers exist as a variety of shapes which would have preferential scattering axes (e.g., rods and prisms) and we may be observing this fact. This anisotropic scattering would not be expected from spherical nanoparticles such as the solid Au nanoparticles. However, the weak SERS population for Au nanoparticles has a similar polarization dependence to the strong SERS population. Interestingly, additional experiments with a commercial preparation of Au nanoparticles (BBI International, 60 nm), did not produce any detectable SERS or Rayleigh signals until aggregation was induced by adding NaCl. These observations suggest that for the spherical Au nanoparticles, the weak SERS population consists of clusters of nanoparticles, and may be different from the case of the Ag nanoparticles.

For the Ag nanoparticles, the strong SERS population formed upon addition of MBA. However, for the Au nanoparticles, the strong SERS population was present without MBA, but at lower I_{Rm}/I_{bkgd}—the strong "SERS" signal in this case is from the continuum background. These clusters appear to have been formed prior to addition of MBA, although there was an increase in size of the clusters upon addition of MBA. The Au nanoparticle clusters were determined to have a larger size and a smaller rotational diffusion component. Additionally, the preferred axes for Rayleigh and Raman scattering did not always overlap, as indicated by the sometimes negative amplitude of the rotational diffusion component. These observations indicate that there were often multiple strong scattering interfaces in each nanoparticle assembly, with one stronger for the Rayleigh signal and another stronger in the Raman signal, and that the Au aggregates may have consisted of more nanoparticle interconnects, appearing rotationally more isotropic than for Ag. For the Ag and Au nanoparticles, the more strongly Raman-active population ("strong SERS population" upper right of Figure 2b−c) showed an increase in the size of nanoparticles due to clustering compared to the weakly Raman-active population ("weak SERS population" bottom middle of Figure 2b−c), as determined from the sizing analysis.

In order to see a significant scattering signal from a nanoparticle, the electric field at the particle must be enhanced compared to the incident electric field both at the laser excitation frequency, g_0 (at ω_0), and at the Raman-shifted frequency, g (at $\omega_0 - \Delta$).[22] We have recently shown that surface-enhanced Raman scattering can be observed even from individual nanoshells,[8] which is mostly due to their relatively strong plasmon resonance, strengthened due to coupling between the inner and outer surfaces of the nanoshell. The plasmon resonances of individual solid Ag and Au nanoparticles in contrast are not strong enough. In order to obtain detectable signals in these cases, interparticle junctions are necessary. Such plasmon resonances of interparticle junctions caused by random aggregation are very difficult to control, which leads to varying spectral characteristics of the plasmon resonance. This lack of control over nanoparticle aggregation causes significantly broader distributions in the ratios I_{Rm}/I_{Ry} and I_{Rm}/I_{bkgd}. It is likely that the large population of solid Au nanoparticles with low I_{Rm}/I_{Ry} represents nanoparticle aggregates that have variable MBA occupation within a large variety of enhancing hot spots—varying plasmon resonance shapes and strengths may play a role. A similar population may exist for the Ag nanoparticles, but the variety of shapes in that sample also may contribute. The hollow nanospheres, however, showed a more uniform response due to the better control over the plasmon resonance.[7]

Conclusion

We have demonstrated the utility of solution-based single-particle techniques for the rapid characterization of the heterogeneity of SERS-active substrates. This valuable tool aids in the rational design of optimized nanoparticle SERS substrates, allowing us to quickly assess a wide range of parameters and determine if there are subpopulations with special properties. We compared several nanoparticle substrates: solid Ag nanoparticles, solid Au nanoparticles, hollow gold nanospheres, and deliberately linked Ag nanoparticles. It is clear that engineered nanostructures produce significantly more consistent SERS response than particles subject to random aggregation, validating these approaches for improv-

(21) Markel, V. A.; Shalaev, V. M.; Zhang, P.; Huynh, W.; Tay, L.; Haslett, T. L.; Moskovits, M. *Phys. Rev. B* **1999**, *59* (16), 10903.

(22) Kerker, M.; Wang, D. S.; Chew, H. *Appl. Opt.* **1980**, *19* (24), 4159–4174.

ing the SERS response of nanoparticle systems. A way to probe the distribution of local field enhancements in SERS substrates using photochemical hole burning (PHB) was recently introduced.[23] The PHB methodology measures the local field enhancements over a wide dynamic range, and can be viewed as complementary to the methodology introduced here. Our methodology obtains a richer data set on SERS substrates that may not withstand PHB laser pulses, albeit over a more limited dynamic range. Our technique should prove useful for examining a variety of SERS and plasmon active architectures for nanosensing applications.

Acknowledgment. This work was performed under the auspices of the U.S. Department of Energy by Lawrence Livermore National Laboratory under Contract DE-AC52-07NA27344. Funding from the Institute for Collaborative Biotechnologies (ICB) through Grant DAAD19-03-D-0004 from U.S. Army Research Office to N. Reich. Support from Lawrence Livermore National Laboratory through a UCDRD grant is gratefully acknowledged. The Center for Biophotonics, an NSF Science and Technology Center, is managed by the University of California, Davis, under Cooperative Agreement No. PHY 0120999.

Supporting Information Available: Extended description of preparation of nanoparticle samples. Description and discussion of simulations of translational and rotational diffusion. This material is available free of charge via the Internet at http://pubs.acs.org.

JA806236K

(23) Fang, Y.; Seong, N.-H.; Dlott, D. D. *Science* **2008**, *321* (5887), 388–392.